

Search for high-frequency gravitational waves with Rydberg atoms

Sugumi Kanno^{*}, Jiro Soda^{b,‡}, and Akira Taniguchi^{*}

^{*}*Department of Physics, Kyushu University, Fukuoka 819-0395, Japan*

^b*Department of Physics, Kobe University, Kobe 657-8501, Japan*

[‡]*International Center for Quantum-field Measurement Systems for Studies of the Universe and Particles (QUP), KEK, Tsukuba 305-0801, Japan*

Abstract

We propose high-frequency gravitational wave (GW) detectors with Rydberg atoms. Rydberg atoms are sensitive detectors of electric fields. By setting up a constant magnetic field, a weak electric field is generated upon the arrival of GWs. The weak electric field signal is then detected by an electromagnetically induced transparency (EIT) in the system of the Rydberg atoms. Recently, the sensitivity of the Rydberg atoms is further improved by combining superheterodyne detection method. Hence, even the weak signal generated by the GWs turns out to be detectable. We calculate the amplitude of Rabi frequency of the Rydberg atoms induced by the GWs and show that the sensitivity of the Rydberg atoms becomes maximum when the size of the Rydberg atoms is close to the wavelength of GWs. As an example, we evaluate the sensitivity of the GW detector with Rubidium Rydberg atoms and find that the detector can probe GWs with a frequency 26.4 GHz and an amplitude of approximately around 10^{-20} . We argue that the sensitivity can be further enhanced by exploiting entangled atoms.

Contents

| | | |
|----------|--|-----------|
| 1 | Introduction | 1 |
| 2 | GW detector with Rydberg atoms | 3 |
| 2.1 | Electric field induced by GWs | 3 |
| 2.2 | Superheterodyne detection strategy | 4 |
| 2.3 | Fermi-normal coordinates | 6 |
| 3 | Sensitivity of GW detectors with Rydberg atoms | 8 |
| 3.1 | Susceptibility and density matrix | 9 |
| 3.2 | Master equation for Rydberg system | 10 |
| 3.3 | Sensitivity of GW detectors with Rydberg atoms | 13 |
| 4 | Conclusion | 17 |
| A | Rabi frequency stemming from GWs | 18 |

1 Introduction

The discovery of gravitational waves (GWs) from a merging black hole binary by LIGO-Virgo Collaboration [1] triggered a new field of science, so-called GW astronomy. As the history of astronomy tells us, it would be crucial to expand the range of observable GW frequency for making further discoveries. Currently, LIGO/Virgo/KAGRA are sensitive to GWs with frequencies only in the range of $10 \sim 10^2$ Hz [2]. The future space-based GW observatories such as LISA [3] and DECIGO [4, 5] will cover the low-frequency band $10^{-4} \sim 10^{-1}$ Hz. Moreover, Pulsar timing arrays are expected to operate in the lower-frequency band $10^{-9} \sim 10^{-7}$ Hz. Recently, it has been reported that the pulsar timing arrays have successfully observed GWs [6, 7, 8, 9, 10, 11, 12, 13, 14]. Thus, GWs in the frequency range from 10^{-9} Hz to 10^2 Hz have been well explored.

On the other hand, observations of GWs at frequencies higher than 10 kHz have not been well developed. This is partially due to a tacit assumption that GWs with a frequency higher than 10 kHz have no relevance to physics. However, the high-frequency GWs associated with

astrophysical phenomena could exist [15, 16]. Moreover, primordial black holes (PBHs) lighter than solar mass can produce GWs with frequencies higher than 10 kHz. We can also expect high-frequency GWs from inflation [17, 18]. The frequency of primordial GWs generated by reheating is typically in the range from MHz to GHz [18]. High-frequency GWs could be generated by cosmological events even after inflation such as the cosmological phase transitions in the early universe [19]. Hence, observations of high-frequency GW will provide information beyond the Standard Model of particle physics (see a review article [20]).

Another reason why GWs with frequencies higher than 10 kHz have not been explored is the presence of obstacles in their detection. Indeed, it is known that the sensitivity of current models of GW detectors becomes worse in the high-frequency range [21]. Hence, it is necessary to come up with new schemes for the detection of GWs at frequencies above 10 kHz. A hint can be obtained by focusing on the similarities between axions and GWs. That is, if axions can be detected, it opens the possibility of detecting GWs as well. Based on this idea, the use of axion detection with magnons provided constraints on high-frequency GWs [22, 23]. This approach can be applied to the interaction between axions and various other excitations, such as axion-photon conversion [24, 25]. Recently, an idea for the detection of axion by using Rydberg atoms was proposed in [26]. Following the strategy mentioned above, we focus on the similarities between axions and GWs, and then see if we can exploit the Rydberg atoms for detecting high-frequency GWs.

Since Rydberg atoms can exhibit very large electric dipole moments [27], they are widely used to measure electric fields as quantum sensors [28]. Indeed, it is possible to measure microwave electric fields over a wide range of frequencies from kHz [29] to THz [30, 31]. The Rydberg atoms can be used as GW detectors because GWs induce a weak electric field when propagating in a homogeneous constant magnetic field. Recently, highly sensitive detection utilizing electromagnetically induced transparency (EIT) with an atomic superheterodyne receiver has been developed [32]. Therefore, it would be worth investigating the possibility of detecting high-frequency GWs with the Rydberg atoms. In particular, the detector with Rydberg atoms has a potential for utilizing quantum entanglement to realize Heisenberg scaling.

The paper is organized as follows. In section 2, we show the electric field can be induced by GWs in the presence of a magnetic field. We also review the basic idea of Rydberg atom

superheterodyne receiver and describe how to use it as a GW detector. Moreover, we review the full-order Fermi normal coordinates for plane GWs. In section 3, we derive the relation between the susceptibility and density matrix of Rydberg atoms. We deduce the density matrix by solving the Lindblad master equation for the system of Rydberg atom. Then, we evaluate the sensitivity of GW detectors with Rydberg atom. We also discuss the possibility of Heisenberg scaling to enhance the sensitivity. The final section is devoted to conclusion. In appendix, the details of calculations for the averaged amplitude of GW are presented. We work in natural unit: $\hbar = c = \varepsilon_0 = \mu_0 = 1$.

2 GW detector with Rydberg atoms

In this section, we propose a method for detecting high-frequency GWs. In the presence of a uniform magnetic field, GWs induce electric fields. The idea is to detect the electric fields by a heterodyne detection method with Rydberg atoms [32].

2.1 Electric field induced by GWs

In this subsection, we derive the electric field induced by GWs. Below we work in the laboratory frame. We consider a situation where GWs propagate in a constant magnetic field. The action we consider is the electromagnetic fields expressed by

$$S = \int d^4x \sqrt{-g} \left[-\frac{1}{4} F^{\mu\nu} F_{\mu\nu} \right] . \quad (2.1)$$

We consider the tensor mode perturbation $h_{\mu\nu}$ in the four-dimensional metric:

$$ds^2 = (\eta_{\mu\nu} + h_{\mu\nu}) dx^\mu dx^\nu , \quad (2.2)$$

where $\eta_{\mu\nu} = \text{diag}(-1, 1, 1, 1)$ represents the Minkowski metric. The indices (μ, ν) run from 0 to 3, and $(0, 1, 2, 3) = (t, x, y, z)$. Substituting Eq. (2.2) into the action (2.1), the action up to the first order in $h_{\mu\nu}$ is given by

$$S = \int d^4x \left[-\frac{1}{4} F^{\mu\nu} F_{\mu\nu} - \frac{1}{4} \left(\frac{1}{2} h F^{\mu\nu} F_{\mu\nu} + h^\nu{}_\alpha F^{\alpha\mu} F_{\mu\nu} - h^\mu{}_\alpha F^{\alpha\nu} F_{\mu\nu} \right) \right] , \quad (2.3)$$

where $F^{\mu\nu} = \partial^\mu A^\nu - \partial^\nu A^\mu$ is the field strength of a gauge field A^μ . The variation of the action (2.3) with respect to the gauge field A^μ gives the Maxwell equation,

$$\partial_\nu F^{\mu\nu} + \partial_\nu \left(\frac{1}{2} h F^{\mu\nu} + h^\nu{}_\alpha F^{\alpha\mu} - h^\mu{}_\alpha F^{\alpha\nu} \right) = 0. \quad (2.4)$$

If we consider the situation that the electric field E^i is induced by the interaction between the constant magnetic field B^i and GWs, then $B^i \sim \mathcal{O}(1)$ and $E^i \sim \mathcal{O}(h)$. Eq. (2.4) at the first order in h becomes

$$\partial_i (E^i - h^0{}_j \varepsilon^{jik} B^k) = 0, \quad (2.5)$$

where we used the relations $F^{0i} = E^i$ and $F^{ij} = \varepsilon^{ijk} B^k$. This can be integrated as

$$E^i - h^0{}_j \varepsilon^{jik} B^k = \varepsilon^{ijk} \partial_j C^k, \quad (2.6)$$

where C^k is an arbitrary constant function. If we impose the initial condition that no electric field is induced without the magnetic field, then $C^i = 0$. Thus, we obtain

$$E^i = \varepsilon^{ijk} h^0{}_j B^k. \quad (2.7)$$

We can naively guess that the magnitude of the induced electric fields is of the order of

$$E^i = 10^{-17} \left(\frac{h}{10^{-20}} \right) \left(\frac{B}{10 \text{ T}} \right) \text{ eV}^2 \sim 10^{-13} \left(\frac{h}{10^{-20}} \right) \left(\frac{B}{10 \text{ T}} \right) \text{ V/cm}. \quad (2.8)$$

Our goal is to study the details of the detection method and clarify if we can detect this tiny electric fields.

2.2 Superheterodyne detection strategy

Rydberg atoms are ultra-sensitive detectors of electric fields. Recently, the authors in [32] proposed a new method to improve the sensitivity further by combining an electromagnetically induced transparency (EIT) method with superheterodyne detection. Indeed, it is now possible to measure the electric field 780 pV/cm with the measurement time 5000 s. This superheterodyne detection utilizes four-level Rydberg atoms, each of which consists of two low energy states $|1\rangle, |2\rangle$ and two Rydberg states $|3\rangle, |4\rangle$ as depicted in Fig.1. The transition from $|1\rangle$ to $|2\rangle$ can be realized by absorbing the probe laser with the frequency corresponding

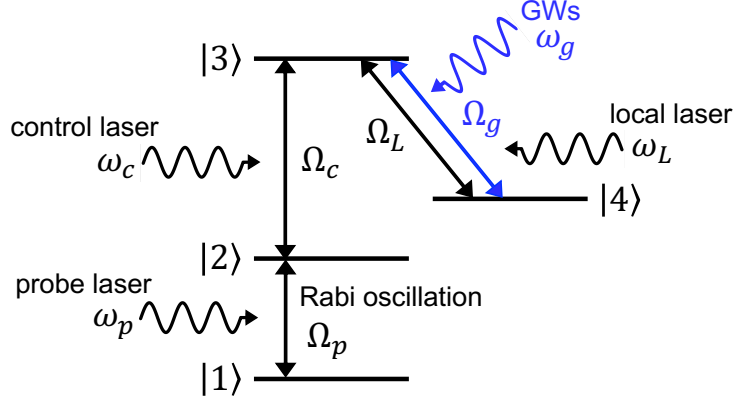


Fig. 1: Energy level of superheterodyne system.

to the energy gap of the two levels $\varepsilon_2 - \varepsilon_1$. The probe laser $\mathbf{E}_p \cos(\omega_p t)$ can induce the Rabi oscillation with the Rabi frequency $\Omega_p \equiv |\mathbf{d}_{12} \cdot \mathbf{E}_p|$. Here, \mathbf{d}_{ij} is the electric dipole moment associated with the transition from $|i\rangle$ to $|j\rangle$. Interestingly, the Rabi oscillation with frequency $\Omega_c \equiv |\mathbf{d}_{23} \cdot \mathbf{E}_c|$ between $|2\rangle$ and $|3\rangle$ driven by the control laser $\mathbf{E}_c \cos(\omega_c t)$ can interfere with the Rabi oscillation between $|1\rangle$ and $|2\rangle$ and then the Rydberg atoms become effectively transparent (no absorption) for the probe laser. As a consequence, the EIT occurs. In the superheterodyne method, another transition between $|3\rangle$ and $|4\rangle$ is driven by the strong local laser $\mathbf{E}_L \cos(\omega_L t)$. In this case, the Rabi frequency is given by $\Omega_L \equiv |\mathbf{d}_{34} \cdot \mathbf{E}_L|$. The point here is that this local strong laser induces splitting of the EIT peak called Autler-Townes splitting [33, 34], that is, splitting of the peak of absorption rate for the probe laser as we will see in Fig. 3. Now, let us suppose that GWs arrive to the Rydberg atoms. If we set up a constant magnetic field away from the four-level Rydberg atoms, then a weak electric field signal with frequency ω_g is generated from the interaction between the GWs and the magnetic field. This electric field induces the Rabi oscillation with the frequency $\Omega_g \equiv |\mathbf{d}_{34} \cdot \mathbf{E}_g|$ between states $|3\rangle$ and $|4\rangle$. As a result, the split absorption rate changes. And this change becomes larger by controlling the local laser as we will see in Eq. (3.30). By splitting the peak of absorption rate of the probe laser in the superheterodyne method, the sensitivity of the signal of the GW turns out to be improved. By using Eq. (2.7), the Rabi frequency induced by the GWs is given by

$$\Omega_g = |\mathbf{d}_{34} \cdot \mathbf{E}| = |d_{34}^i \varepsilon^{ijk} h_j^0 B^k|, \quad (2.9)$$

Note that $\Omega_g \ll \Omega_L$. This induces a change in the absorption rate of the probe laser when the GWs arrive. In this way, a signal of the GWs can be measured by the change of the absorption rate of the probe laser. We also note that this superheterodyne method is proposed by the authors in [26] for the detection of axion fields.

2.3 Fermi-normal coordinates

In the previous subsection, we considered a constant magnetic field in the laboratory frame. In order to measure GWs that appeared in Eq. (2.9) while maintaining the constant magnetic field, it is necessary to introduce a local inertial system for the GWs. We use Fermi-normal (FN) coordinates that describe the effect of gravity from the point of view of an observer in the laboratory. In the FN coordinate, the metric is perturbatively expanded under the condition that the wavelength of the GWs, λ_g , is much longer than the size of detector L , that is, $\lambda_g \gg L$. However, since the detector becomes the most sensitive for $\lambda_g \sim L$, we need to improve the FN coordinates so that they can incorporate shorter wavelengths of the GWs. The authors in [35, 36, 37] made this possible in the case that the GW is a plane wave. Recently, the authors in [38] made use of the improved FN coordinate to detect high-frequency GWs with microwave cavities. It is also shown that the sensitivity of magnon GW detectors can be improved by using the FN coordinates [39]. If we assume that the GW is described by the plane wave $h \propto e^{-i(\omega_g t - \mathbf{k} \cdot \mathbf{x})}$, the metric components in the FN coordinates are found to be

$$g_{00} = -1 - R_{0i0j}(0)x^i x^j \times 2 \operatorname{Re} \left[-\frac{i}{\mathbf{k} \cdot \mathbf{x}} + \frac{1 - e^{-i\mathbf{k} \cdot \mathbf{x}}}{(\mathbf{k} \cdot \mathbf{x})^2} \right], \quad (2.10)$$

$$g_{0i} = -\frac{2}{3}R_{0jik}(0)x^j x^k \times 3 \operatorname{Re} \left[-\frac{i}{2(\mathbf{k} \cdot \mathbf{x})} - \frac{e^{-i\mathbf{k} \cdot \mathbf{x}}}{(\mathbf{k} \cdot \mathbf{x})^2} - i\frac{1 - e^{-i\mathbf{k} \cdot \mathbf{x}}}{(\mathbf{k} \cdot \mathbf{x})^3} \right], \quad (2.11)$$

$$g_{ij} = \delta_{ij} - \frac{1}{3}R_{ikjl}(0)x^k x^l \times 6 \operatorname{Re} \left[-\frac{1 + e^{-i\mathbf{k} \cdot \mathbf{x}}}{(-\mathbf{k} \cdot \mathbf{x})^2} - 2i\frac{1 - e^{-i\mathbf{k} \cdot \mathbf{x}}}{(\mathbf{k} \cdot \mathbf{x})^3} \right], \quad (2.12)$$

where x^i are spatial coordinates, $k^i x_i = \mathbf{k} \cdot \mathbf{x}$ and $R_{\mu\nu\rho\sigma}(0)$ is the Riemann tensor evaluated at the origin $x^i = 0$. In order to evaluate Eq. (2.7), we focus on Eq. (2.11). Since the Riemann tensor in Eq. (2.11) is gauge invariant at the linear order, we can express it by the metric in the transverse-traceless (TT) gauge. Then, Eq. (2.11) in the TT gauge, h_{0i} , is calculated as

$$h_{0i} = \omega_g \left(k_k h_{ji}^{\text{TT}} \Big|_{\mathbf{x}=0} x^j x^k - k_i h_{jk}^{\text{TT}} \Big|_{\mathbf{x}=0} x^j x^k \right) \left[\frac{\cos(\mathbf{k} \cdot \mathbf{x})}{(\mathbf{k} \cdot \mathbf{x})^2} - \frac{\sin(\mathbf{k} \cdot \mathbf{x})}{(\mathbf{k} \cdot \mathbf{x})^3} \right]. \quad (2.13)$$

Let us assume that the uniform magnetic field \mathbf{B} is pointing only in the positive z direction. Without loss of generality, we can consider the GWs propagating in the z - x plane and its wave vector is given by $\mathbf{k} = k(\sin \theta, 0, \cos \theta)$. Then, the polarization tensors $e_{ij}^{(+)}, e_{ij}^{(\times)}$ are expressed as

$$e_{ij}^{(+)} = \frac{1}{\sqrt{2}} \begin{pmatrix} \cos^2 \theta & 0 & -\cos \theta \sin \theta \\ 0 & -1 & 0 \\ -\cos \theta \sin \theta & 0 & \sin^2 \theta \end{pmatrix}, \quad e_{ij}^{(\times)} = \frac{1}{\sqrt{2}} \begin{pmatrix} 0 & \cos \theta & 0 \\ \cos \theta & 0 & -\sin \theta \\ 0 & -\sin \theta & 0 \end{pmatrix} \quad (2.14)$$

The GWs are then expanded in the form of circularly polarized monochromatic plane-wave,

$$h_{ij}^{\text{TT}}(t, \mathbf{x}) = h^{(+)} e_{ij}^{(+)} \cos(\omega t - \mathbf{k} \cdot \mathbf{x}) + h^{(\times)} e_{ij}^{(\times)} \cos(\omega t - \mathbf{k} \cdot \mathbf{x}), \quad (2.15)$$

where $h^{(+)}$ and $h^{(\times)}$ are the amplitude of the GWs. Substituting Eq. (2.15) into Eq. (2.13), we find

$$h_{0x} = \omega_g k \frac{h^{(+)}}{\sqrt{2}} \sin \theta (y^2 - z^2) \left[\frac{\cos(\mathbf{k} \cdot \mathbf{x})}{(\mathbf{k} \cdot \mathbf{x})^2} - \frac{\sin(\mathbf{k} \cdot \mathbf{x})}{(\mathbf{k} \cdot \mathbf{x})^3} \right], \quad (2.16)$$

$$h_{0y} = \omega_g k \frac{h^{(\times)}}{\sqrt{2}} \cos \theta \sin \theta (x^2 - z^2) \left[\frac{\cos(\mathbf{k} \cdot \mathbf{x})}{(\mathbf{k} \cdot \mathbf{x})^2} - \frac{\sin(\mathbf{k} \cdot \mathbf{x})}{(\mathbf{k} \cdot \mathbf{x})^3} \right], \quad (2.17)$$

where we ignored the terms involving $x^j x^k = xy, yz, zx$ in Eq. (2.13) because they vanish when averaging h_{0i} over the size of detector. Let's say the size of the detector consisting of the Rydberg atoms is L . We average Eqs. (2.16) and (2.17) over the size of detector radius $\ell = L/2$ in spherical coordinates (r, ζ, ϕ) . The details of the calculations are presented in the Appendix A where we introduced a dimensionless parameter $\epsilon = \ell/\lambda_g = k\ell/(2\pi)$ and a variable $r' = r/\ell$. The spherically-averaged h_{0i} over the size of detector is given in the form

$$\langle h_{0x} \rangle = \frac{h^{(+)}}{\sqrt{2}} \sin \theta F(\epsilon), \quad (2.18)$$

$$\langle h_{0y} \rangle = \frac{h^{(\times)}}{\sqrt{2}} \cos \theta \sin \theta F(\epsilon), \quad (2.19)$$

where we used $\omega_g = k$ and defined $F(\epsilon)$ as

$$F(\epsilon) \equiv \frac{\pi(\pi^2 \epsilon^2 - 3) \text{Si}(2\pi\epsilon)}{2\pi\epsilon} + \frac{\pi(2\pi^2 \epsilon^2 - 15) \cos(2\pi\epsilon)}{8\pi^2 \epsilon^2} + \frac{\pi(2\pi^2 \epsilon^2 + 15) \sin(2\pi\epsilon)}{16\pi^3 \epsilon^3}. \quad (2.20)$$

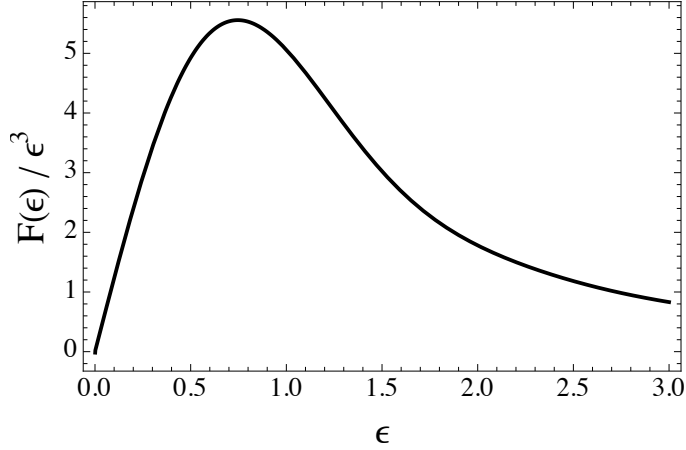


Fig. 2: The plot of $F(\epsilon)/\epsilon^3$ as a function of $\epsilon = \ell/\lambda_g = k\ell/(2\pi) = \omega_g\ell/(2\pi)$, which takes the maximum at $\epsilon \sim 0.7$.

Here, $\text{Si}(\epsilon)$ is the sine integral defined as $\text{Si}(x) = \int_0^x dt \sin t/t$. We plotted $F(\epsilon)/\epsilon^3$ as a function of ϵ in Fig. 2. Finally, the averaged Rabi frequency Ω_g is calculated such as

$$\begin{aligned} \langle \Omega_g \rangle &= \langle |\mathbf{d}^{(34)} \cdot \mathbf{E}| \rangle = |d^{(3,4)i} \epsilon^{ijk} \langle h^0_j \rangle B^k| \\ &= F(\epsilon) \frac{B_z}{\sqrt{2}} \left| \sin \theta \left[d_x^{(34)} h^{(\times)} \cos \theta - d_y^{(34)} h^{(+)} \right] \right|. \end{aligned} \quad (2.21)$$

For long-wavelength GWs ($\epsilon \ll 1$), the sensitivity of the detector to the GWs is significantly reduced due to the rapid decay of $F(\epsilon)$ as shown in Fig. 2. This reflects the equivalence principle for the detector. On the other hand, for short-wavelength GWs ($\epsilon \gg 1$), $F(\epsilon)$ increases as $F(\epsilon) \propto \epsilon$. However, as the wavelength of the GWs becomes shorter, the number of Rydberg atoms within the wavelength decreases at a rate proportional to its volume ϵ^{-3} . Hence, the sensitivity is reduced by ϵ^{-3} . As a result, the sensitivity of the detector is maximized at $\epsilon \sim 0.7$.

3 Sensitivity of GW detectors with Rydberg atoms

In this section, we evaluate the sensitivity of the GW detector with heterodyne receivers. A signal of the GWs is measured by a change in the absorption rate of the probe laser. It is known that the absorption rate is proportional to the imaginary part of electric susceptibility

which can be related to the density operator of an atom [40]. After briefly reviewing those basics, we derive the SNR (signal to noise ratio) of the GW detector.

3.1 Susceptibility and density matrix

First, we show that the absorption rate is proportional to the imaginary part of electric susceptibility. Let us consider the electric field of a plane electromagnetic wave traveling in the z -direction

$$E(z, t) = E_0 \exp(ikz - i\omega t), \quad (3.1)$$

where E_0 is the amplitude. Complex relative permittivity is expressed as

$$\varepsilon(\omega, k) = 1 + \chi(\omega, k), \quad (3.2)$$

where $\chi(\omega, k)$ is the linear susceptibility and $|\chi| \ll 1$. We can introduce the refractive index $n(\omega)$ and the extinction coefficient $\kappa(\omega)$ by separating $\sqrt{\varepsilon(k, \omega)}$ into its real and imaginary parts such as

$$\sqrt{\varepsilon(k, \omega)} = \frac{k}{\omega} \equiv n(\omega) + i\kappa(\omega). \quad (3.3)$$

Then Eq. (3.1) is written as

$$E(z, t) = E_0 \exp[i(\omega n(\omega)z - \omega t)] \exp[-\omega\kappa(\omega)z]. \quad (3.4)$$

Note that $\kappa(\omega)$ gives an exponential decay of the electric field, so it is referred to as absorption rate. Next, we write the susceptibility with real and imaginary parts χ' and χ'' as follows.

$$\chi \equiv \chi' + i\chi''. \quad (3.5)$$

Substituting Eq. (3.5) into Eqs. (3.2) and (3.3), we find

$$\kappa(\omega) = \frac{\chi''}{2}. \quad (3.6)$$

This shows that the absorption rate is proportional to the imaginary part of susceptibility.

Next, we derive the relation between the susceptibility and density matrix of an atom. Let us focus on a two-level system $|1\rangle$ and $|2\rangle$ of an atom. The dipole moment operator is given by

$$\hat{\mathbf{d}}_{12} = \mathbf{d}_{12} |1\rangle \langle 2| + \mathbf{d}_{21} |2\rangle \langle 1|, \quad (3.7)$$

where \mathbf{d}_{12} is the dipole moment. In the semiclassical theory, the polarization \mathbf{P} at the position of an atom induced by a probe laser $\mathbf{E}_p \cos(\omega_p t)$ is expressed as $\mathbf{P}(t) = N \text{Tr}[\hat{\mathbf{d}}\rho(t)]$, where N is the atom number density and $\rho(t)$ is the density operator of the atom. Combining this with Eq. (3.7), we have

$$\mathbf{P}(t) = N\mathbf{d}_{12}\rho_{21}(t) + \text{c.c.} . \quad (3.8)$$

If we decompose the polarization $\mathbf{P}(t)$ into Fourier modes, we have

$$\mathbf{P}(t) = \tilde{\mathbf{P}}(\omega_p)e^{-i\omega_p t} + \text{c.c.} . \quad (3.9)$$

where $\tilde{\mathbf{P}}(\omega_p)$ is the Fourier transform of $\mathbf{P}(t)$. By comparing Eq. (3.8) with Eq. (3.9), we find

$$\tilde{\mathbf{P}}(\omega_p) = N\mathbf{d}_{12}\rho_{21}(t)e^{i\omega_p t} . \quad (3.10)$$

Similarly, the electric field $\mathbf{E}(t) = \mathbf{E}_p \cos(\omega_p t)$ is decomposed into Fourier mode

$$\mathbf{E}(t) = \tilde{\mathbf{E}}(\omega_p)e^{-i\omega_p t} + \text{c.c.} = \frac{1}{2}\mathbf{E}_p e^{-i\omega_p t} + \text{c.c.} \quad (3.11)$$

with $\tilde{\mathbf{E}}(\omega_p)$ being the Fourier transform of $\mathbf{E}(t)$. Note that we used $\cos(\omega_p t) = (e^{i\omega_p t} + e^{-i\omega_p t})/2$ in the second equality. The susceptibility is defined by

$$\tilde{\mathbf{P}}(\omega_p) = \chi(\omega_p)\tilde{\mathbf{E}}(\omega_p) . \quad (3.12)$$

So if we use Eqs. (3.10), (3.11) and (3.12), the susceptibility is found to be related to the density operator of the atom

$$\chi(\omega_p) = \frac{2N|\mathbf{d}_{12}|^2}{\Omega_p}\rho_{21}(t)e^{i\omega_p t} . \quad (3.13)$$

3.2 Master equation for Rydberg system

As we explained in Sec. 2.2, we consider a four-level Rydberg atom that consists of two low energy states $|1\rangle$, $|2\rangle$ and two Rydberg states $|3\rangle$, $|4\rangle$ as depicted in Fig.1. The total Hamiltonian $\hat{H}(t)$ for the four-level atom interacting with probe laser, control laser, strong local laser and GWs is written as

$$\hat{H}(t) = \hat{H}_0 + \hat{H}'(t) , \quad (3.14)$$

with the unperturbed Hamiltonian

$$\hat{H}_0 = \varepsilon_1 |1\rangle \langle 1| + \varepsilon_2 |2\rangle \langle 2| + \varepsilon_3 |3\rangle \langle 3| + \varepsilon_4 |4\rangle \langle 4| , \quad (3.15)$$

where ε_i with $i = 1, 2, 3, 4$ denote the level energies, and with the dipole interaction Hamiltonian

$$\hat{H}'(t) = -\frac{\Omega_p}{2} e^{-i\omega_p t} |2\rangle \langle 1| - \frac{\Omega_c}{2} e^{-i\omega_c t} |3\rangle \langle 2| - \left(\frac{\Omega_L}{2} e^{-i\omega_L t} + \frac{\Omega_g}{2} e^{-i\omega_g t} \right) |3\rangle \langle 4| + \text{h.c.} , \quad (3.16)$$

where Ω_p , Ω_c , Ω_L , and Ω_g , are Rabi frequencies associated with the coupling of the lasers of frequencies ω_p , ω_c , ω_L and ω_g to the atomic transitions $|1\rangle \rightarrow |2\rangle$, $|2\rangle \rightarrow |3\rangle$ and $|3\rangle \rightarrow |4\rangle$, respectively. It is convenient to transform the Hamiltonian to a rotating frame by using

$$\hat{\mathcal{H}} = \hat{U} \hat{H} \hat{U}^\dagger - i \hat{U} \frac{d}{dt} \hat{U}^\dagger , \quad (3.17)$$

with the unitary operator

$$\begin{aligned} \hat{U} \equiv & \exp \left[i\varepsilon_1 |1\rangle \langle 1| t + i(\varepsilon_1 + \omega_p) |2\rangle \langle 2| t \right. \\ & \left. + i(\varepsilon_1 + \omega_p + \omega_c) |3\rangle \langle 3| t + i(\varepsilon_1 + \omega_p + \omega_c - \omega_L) |4\rangle \langle 4| t \right] . \end{aligned} \quad (3.18)$$

Then, the Hamiltonian in the rotating frame is written by

$$\begin{aligned} \hat{\mathcal{H}} = & \Delta_p |2\rangle \langle 2| + (\Delta_p + \Delta_c) |3\rangle \langle 3| + (\Delta_p + \Delta_c + \Delta_L) |4\rangle \langle 4| \\ & + \left[-\frac{\Omega_p}{2} |2\rangle \langle 1| - \frac{\Omega_c}{2} |3\rangle \langle 2| - \frac{\Omega_L + \Omega_g e^{-i\delta_g t}}{2} |3\rangle \langle 4| + \text{h.c.} \right] , \end{aligned} \quad (3.19)$$

where we defined detunings between the lasers and atomic frequencies as Δ_p , Δ_c , Δ_L , and δ_g , which are expressed by

$$\Delta_p \equiv (\varepsilon_2 - \varepsilon_1) - \omega_p , \quad (3.20)$$

$$\Delta_c \equiv (\varepsilon_3 - \varepsilon_2) - \omega_c , \quad (3.21)$$

$$\Delta_L \equiv \omega_L - (\varepsilon_3 - \varepsilon_4) , \quad (3.22)$$

$$\delta_g \equiv \omega_g - \omega_L . \quad (3.23)$$

Note that the time dependence except for δ_g in the Hamiltonian was removed in this rotating frame.

The Lindblad master equation for total system's density matrix in the rotating frame $\tilde{\rho}$ is given by

$$\frac{d}{dt}\tilde{\rho} = -i[\hat{\mathcal{H}}, \tilde{\rho}] + \sum_{k=2,3,4} \gamma_k \left[\hat{O}_k \tilde{\rho} \hat{O}_k^\dagger - \frac{1}{2} \{ \hat{O}_k^\dagger \hat{O}_k, \tilde{\rho} \} \right], \quad (3.24)$$

where $\hat{O}_k = |1\rangle \langle k|$ represents the relaxation process in the atom.

In order to solve the master equation (3.24), we use linear approximation under the assumption that the frequency of the Rabi oscillation Ω_p is small enough. Then we can assume that the atom is in stationary state where an electron is in the ground state initially. That is, the initial condition becomes $\tilde{\rho}_{11}(0) = 1$, $\tilde{\rho}_{12}(0) = \tilde{\rho}_{13}(0) = \tilde{\rho}_{14}(0) = \tilde{\rho}_{22}(0) = \tilde{\rho}_{23}(0) = \tilde{\rho}_{24}(0) = \tilde{\rho}_{33}(0) = \tilde{\rho}_{34}(0) = \tilde{\rho}_{44}(0) = 0$. And we can regard $\tilde{\rho}_{11} = \Omega_c = \Omega_L = \Omega_g = \mathcal{O}(1)$, $\tilde{\rho}_{12} = \tilde{\rho}_{13} = \tilde{\rho}_{14} = \tilde{\rho}_{22} = \tilde{\rho}_{23} = \tilde{\rho}_{24} = \mathcal{O}(\Omega_p)$. Under these assumptions, master equations become

$$\frac{d}{dt}\tilde{\rho}_{21} = -\left(\frac{\gamma_2}{2} + i\Delta_p\right)\tilde{\rho}_{21} + i\frac{\Omega_p}{2}\tilde{\rho}_{11} + i\frac{\Omega_c}{2}\tilde{\rho}_{31}, \quad (3.25)$$

$$\frac{d}{dt}\tilde{\rho}_{31} = -\left(\frac{\gamma_3}{2} + i(\Delta_p + \Delta_c)\right)\tilde{\rho}_{31} + i\frac{\Omega_c}{2}\tilde{\rho}_{21} + i\frac{\Omega}{2}\tilde{\rho}_{41}, \quad (3.26)$$

$$\frac{d}{dt}\tilde{\rho}_{41} = -\left(\frac{\gamma_4}{2} + i(\Delta_p + \Delta_c + \Delta_L)\right)\tilde{\rho}_{41} + i\frac{\Omega}{2}\tilde{\rho}_{31}, \quad (3.27)$$

where we introduced $\Omega \equiv \Omega_L + \Omega_g e^{-i\delta_g t}$ and the relation $\Omega_g \ll \Omega_L$ allows us to regard Ω as a constant. The stationary state solution of these equations $\tilde{\rho}_{21}^{\text{st}}$ is

$$\tilde{\rho}_{21}^{\text{st}} = \frac{AC + BD}{A^2 + B^2}\Omega_p + i\frac{AD - BC}{A^2 + B^2}\Omega_p, \quad (3.28)$$

where we defined A , B , C , and D as

$$A \equiv 4(\Delta_p + \Delta_c + \Delta_L)(\gamma_3\Delta_p + \gamma_2(\Delta_p + \Delta_c)) - \gamma_2(\gamma_3\gamma_4 + \Omega^2) + \gamma_4(4\Delta_p^2 + 4\Delta_c\Delta_p - \Omega_c^2),$$

$$B \equiv 2(\Delta_p + \Delta_c + \Delta_L)(4\Delta_p^2 + 4\Delta_p\Delta_c - \Omega_c^2 - \gamma_2\gamma_3) - 2\gamma_3\gamma_4\Delta_p - 2\gamma_2\gamma_4(\Delta_p + \Delta_c) - 2\Delta_p\Omega^2,$$

$$C \equiv 2\gamma_3(\Delta_p + \Delta_c + \Delta_L) + 2\gamma_4(\Delta_p + \Delta_c),$$

$$D \equiv 4(\Delta_p + \Delta_c + \Delta_L)(\Delta_p + \Delta_c) - \gamma_3\gamma_4 - \Omega^2.$$

This result $\tilde{\rho}_{21}^{\text{st}}$ in the rotating frame has to be transformed back to ρ_{21} in the original frame by using $\rho_{21}(t) = \tilde{\rho}_{21}(\omega_p)e^{-i\omega_p t}$. Then substituting the $\rho_{21}(t)$ into Eq. (3.13), we finally

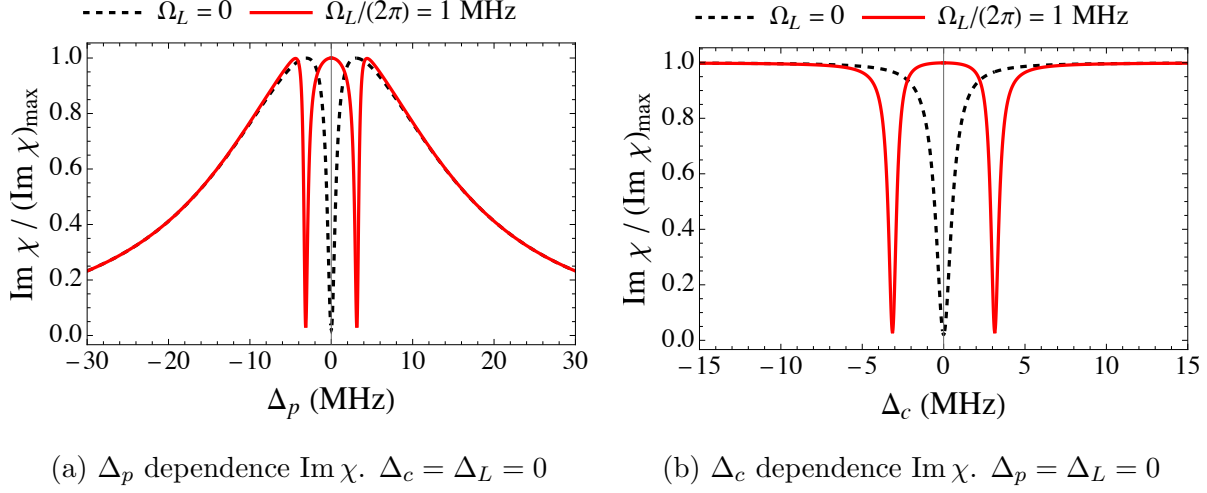


Fig. 3: The plot of the Δ_p or Δ_c dependence of $\text{Im } \chi$. Here we used $\gamma_2/(2\pi) = 5.2$ MHz, $\gamma_3/(2\pi) = 3.9$ kHz, $\gamma_4/(2\pi) = 1.7$ kHz, $\Omega_p/(2\pi) = 5.7$ MHz, $\Omega_c/(2\pi) = 0.97$ MHz, $\Omega_L/(2\pi) = 1.0$ MHz [32]. $\text{Im } \chi / (\text{Im } \chi)_{\text{max}}$ represents the absorption rate of the probe laser. The local strong laser induces the Autler-Townes splitting.

obtain the absorption rate in terms of the imaginary part of susceptibility in the form

$$\text{Im } \chi = 2N|\mathbf{d}_{12}|^2 \frac{AD - BC}{A^2 + B^2}. \quad (3.29)$$

3.3 Sensitivity of GW detectors with Rydberg atoms

For instance, let us consider the resonance condition $\Delta_L = 0$ between $|3\rangle$ and $|4\rangle$. We can assume that $\gamma_3 = \gamma_4 = 0$ because the relations $\gamma_3, \gamma_4 \ll \gamma_2$ hold in general. To evaluate the sensitivity, we restore the time-dependent term in Ω in Eq. (3.29). We first expand $|\Omega|^2$ up to the first order in Ω_g such as $|\Omega|^2 = (\Omega_L + \Omega_g e^{-i\delta_g t})(\Omega_L + \Omega_g e^{i\delta_g t}) \sim \Omega_L^2 + 2\Omega_L\Omega_g \cos \delta_g t$, then plugging it into Eq. (3.29), we find

$$\text{Im } \chi = 2N|\mathbf{d}_{12}|^2 \kappa_0 + 2N|\mathbf{d}_{12}|^2 \kappa_1 \Omega_g \cos(\delta_g t) \quad (3.30)$$

where κ_0 and κ_1 are respectively calculated as

$$\begin{aligned}
\kappa_0 &= \frac{1}{\Omega_p} \text{Im} \rho_{12} (\Omega_L^2) \\
&= \frac{\gamma_2 [4(\Delta_p + \Delta_c)^2 - \Omega_L^2]^2}{\gamma_2^2 [4(\Delta_p + \Delta_c)^2 - \Omega_L^2]^2 + 4 [4\Delta_p (\Delta_p + \Delta_c)^2 - (\Delta_p + \Delta_c) \Omega_c^2 - \Delta_p \Omega_L^2]^2}, \\
\kappa_1 &= 2 \frac{\Omega_L}{\Omega_p} \left. \frac{d \text{Im} \rho_{12}(x)}{dx} \right|_{x=\Omega_L^2} \\
&= \frac{16\gamma_2 \Omega_c^2 \Omega_L (\Delta_p + \Delta_c) [4(\Delta_p + \Delta_c)^2 - \Omega_L^2] [4\Delta_p (\Delta_p + \Delta_c)^2 - (\Delta_p + \Delta_c) \Omega_c^2 - \Delta_p \Omega_L^2]}{\left[\gamma_2^2 [4(\Delta_p + \Delta_c)^2 - \Omega_L^2]^2 + 4 [4\Delta_p (\Delta_p + \Delta_c)^2 - (\Delta_p + \Delta_c) \Omega_c^2 - \Delta_p \Omega_L^2]^2 \right]^2}.
\end{aligned}$$

Note that κ_1 represents a change of absorption rate of the probe laser when the GWs arrived. Since the κ_1 is proportional to Ω_L , we see the change is enhanced by the control of the local laser.

By using Eqs. (3.4) and (3.6), the output power of the probe laser $P(t)$ is calculated as $P(t) = |E(z, t)|^2 = |E_0|^2 e^{-2\omega_p \kappa z} = P_i e^{-\omega_p L \text{Im} \chi}$, where $P_i (= |E_0|^2)$ is input power of the probe laser, L is the size of Rydberg atoms and we set $n = 1$, $z = L$. Substituting Eq. (3.30) into the $P(t)$, we find

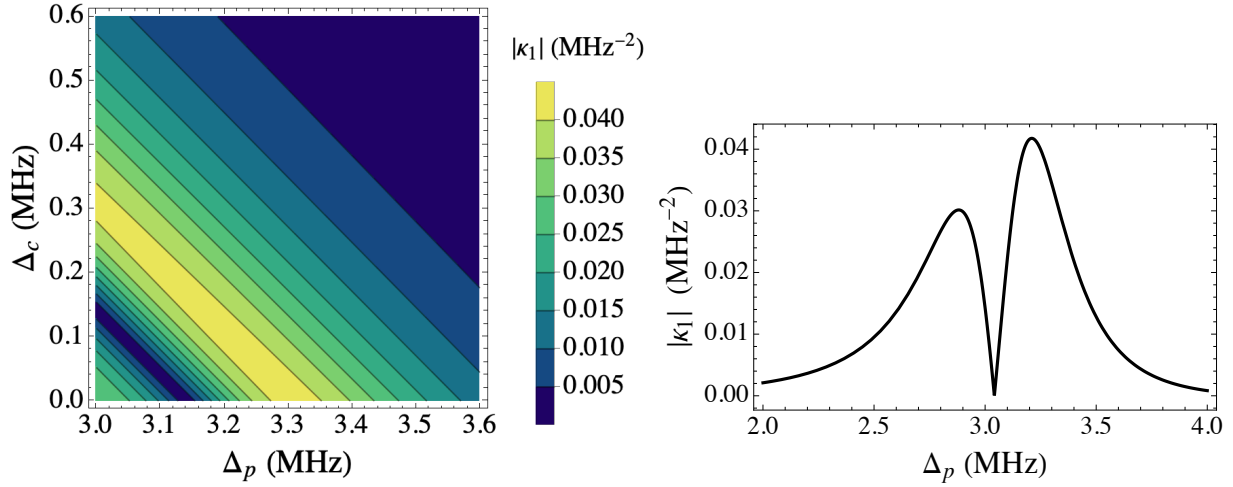
$$\begin{aligned}
P(t) &= P_i e^{-\omega_p L 2N |\mathbf{d}_{12}|^2 \kappa_0} e^{-\omega_p L 2N |\mathbf{d}_{12}|^2 \kappa_1 \Omega_g \cos(\omega_g t)} \\
&\approx P_i e^{-\omega_p L 2N |\mathbf{d}_{12}|^2 \kappa_0} - P_i e^{-\omega_p L 2N |\mathbf{d}_{12}|^2 \kappa_0} \cdot 2N |\mathbf{d}_{12}|^2 \omega_p L \kappa_1 \Omega_g \cos(\omega_g t) \\
&\equiv P_0 + 2P_0 N |\mathbf{d}_{12}|^2 \omega_p L \kappa_1 \Omega_g \cos(\delta_g t), \tag{3.31}
\end{aligned}$$

where $P_0 \equiv P_i e^{-\omega_p L 2N |\mathbf{d}_{12}|^2 \kappa_0}$. Now, SNR (signal to noise ratio) can be defined as the ratio of the output power with a signal of GWs to that with no signal of GWs, that is, the ratio of the second term to the first term in Eq. (3.31):

$$\text{SNR} \equiv 2N |\mathbf{d}_{12}|^2 \omega_p L |\kappa_1| \Omega_g. \tag{3.32}$$

Using the SNR, we can estimate the sensitivity of detector with the Rydberg atoms, that is, the minimum measurable value of the electric field when the GWs arrived. A minimum detectable signal is given by $\text{SNR} = 1$, which corresponds to $\Omega_g = 1/(2N |\mathbf{d}_{12}|^2 \omega_p L |\kappa_1|)$. Combining it with the relation $\Omega_g = |\mathbf{d}_{34} \cdot \mathbf{E}_{\min}|$, we have

$$E_{\min} = \frac{\Omega_g}{|\mathbf{d}_{34}|} = \frac{1}{2 |\mathbf{d}_{34}| |\mathbf{d}_{12}|^2 N \omega_p L |\kappa_1|}. \tag{3.33}$$



(a) Δ_p and Δ_c dependence of $|\kappa_1|$.

(b) Δ_p dependence of $|\kappa_1|$. $\Delta_c = 0.1$ MHz

Fig. 4: The plot of detuning Δ_p and Δ_c dependence of $|\kappa_1|$. Parameters are $\Delta_L=0$, $\gamma_2/(2\pi) = 5.2$ MHz, $\gamma_3 = \gamma_4 = 0$, $\Omega_p/(2\pi) = 5.7$ MHz, $\Omega_c/(2\pi) = 0.97$ MHz, $\Omega_L/(2\pi) = 1.0$ MHz. At $\Delta_p = 3.2$ MHz and $\Delta_c = 0.1$ MHz, $|\kappa_1|$ become maximum which is $|\kappa_1| = 0.042$ MHz⁻², where sensitivity becomes best.

We see that sensitivity of the detector with the Rydberg atoms for the GWs becomes higher as $|\kappa_1|$ becomes larger. To show the maximum value of $|\kappa_1|$, the detuning dependence of $|\kappa_1|$ is plotted in Fig. 4. $|\kappa_1|$ has a maximum value of 0.042 MHz⁻², where the sensitivity is maximum.

Let us estimate the minimum measurable value. We consider Rubidium atoms with the four levels $|1\rangle : 5S_{1/2}$, $|2\rangle : 5P_{3/2}$, $|3\rangle : 59P_{3/2}$, and $|4\rangle : 57D_{5/2}$. In this case, the dipole moment and the energy gap are calculated as $|\mathbf{d}_{12}| = 5.158ea_0$, $\varepsilon_2 - \varepsilon_1 = 384$ THz, $|\mathbf{d}_{34}| = 2416ea_0$, and $\varepsilon_3 - \varepsilon_4 = 26.4$ GHz. Here, e is a electric charge and a_0 is the Bohr radius, and we used Alkali Rydberg Calculator (ARC) package [41] to calculate the dipole moment. According to [42], N can be increased up to $N \sim 1.6 \times 10^{14}$ cm⁻³. The size of the Rydberg atoms is $L = 2\ell = 10$ cm. Thus, we obtain

$$\begin{aligned}
 E_{\min} = & 1.5 \times 10^{-16} \text{ eV}^2 \left(\frac{2416 ea_0}{|\mathbf{d}_{34}|} \right) \left(\frac{5.158 ea_0}{|\mathbf{d}_{12}|} \right)^2 \left(\frac{1.6 \times 10^{14} \text{ cm}^{-3}}{N} \right) \\
 & \times \left(\frac{384 \text{ THz}}{\omega_p} \right) \left(\frac{10 \text{ cm}}{L} \right) \left(\frac{0.042 \text{ MHz}^{-2}}{|\kappa_1|} \right). \quad (3.34)
 \end{aligned}$$

The minimum detectable electric fields turn out to be $E_{\min} = 1.5 \times 10^{-16} \text{ eV}^2 = 2.3 \text{ pV/cm}$.

Next we estimate the amplitude of the measurable GWs. In Eq. (2.21), to consider the situation of maximum sensitivity, we choose $\theta = \pi/2$ that represents the GW is perpendicular to the magnetic field. In this case, from Eqs. (2.21) and (3.33), h is expressed as

$$h = \frac{\sqrt{2} \langle \Omega_g \rangle}{|\mathbf{d}_{34}| B_z F(\epsilon)} = \frac{\sqrt{2}}{2} \frac{1}{B_z F(\epsilon) |\mathbf{d}_{34}| |\mathbf{d}_{12}|^2 N \omega_p L |\kappa_1|}. \quad (3.35)$$

Here, we take $B_z = 10 \text{ T}$. The energy gap of the two Rydberg states determines the measurable frequency of the GWs, so $\omega_g \sim \varepsilon_4 - \varepsilon_3 = 26.4 \text{ GHz}$, which corresponds to the wavelength $\lambda_g = 1.14 \text{ cm}$. When the size of the Rydberg atoms is $L = 2\ell = 10 \text{ cm}$, then the value of $F(\epsilon)$ at $\epsilon = \omega_g \ell / 2\pi = 0.701$ becomes $F(0.701) \simeq 1.91$. Thus, the detectable amplitude of the GWs by using the Rydberg atoms turns out to be

$$h = 5.7 \times 10^{-20} \left(\frac{1.91}{F(\epsilon)} \right) \left(\frac{10 \text{ T}}{B_z} \right) \left(\frac{2416 \text{ ea}_0}{|\mathbf{d}_{34}|} \right) \left(\frac{5.158 \text{ ea}_0}{|\mathbf{d}_{12}|} \right)^2 \left(\frac{1.6 \times 10^{14} \text{ cm}^{-3}}{N} \right) \\ \times \left(\frac{384 \text{ THz}}{\omega_p} \right) \left(\frac{10 \text{ cm}}{L} \right) \left(\frac{0.042 \text{ MHz}^{-2}}{|\kappa_1|} \right). \quad (3.36)$$

Finally, let us estimate the sensitivity achievable in the quantum projection noise limit. The basic idea of the EIT is to measure the frequency shift between split two peaks $\Delta\nu$ which is related to the amplitude of electric field E and electric dipole moment d as

$$E \simeq \frac{\Delta\nu}{d}. \quad (3.37)$$

Since $\Delta\nu \sim 1/(\sqrt{n} T_2)$, where T_2 is the coherence time of the EIT and n is the number of independent measurement taking place per second, we obtain

$$E \simeq \frac{1}{d\sqrt{n} T_2}. \quad (3.38)$$

Let T be the integration time of the coherent EIT process. Then, we can deduce

$$n = N_a \frac{T}{T_2}, \quad (3.39)$$

where N_a is the number of atoms participating in the measurement per second. Hence, the measurable electric field in the quantum projection noise limit (QP NL) is given by

$$E_{\text{QP NL}} = \frac{1}{d\sqrt{N_a T T_2}}. \quad (3.40)$$

The dipole moment is $d = |\mathbf{d}_{34}| = 2416ea_0 \sim 3.87 \times 10^{-6}$ cm. The number of atoms participating in the measurement is $N_a = 2.14 \times 10^{13} \text{ s}^{-1}$ [32], and the coherence time of Rydberg atom EIT system is $T_2 = 100$ ns [42]. Thus, we obtain

$$E_{\text{QPNL}} = 1.7 \times 10^{-1} \text{ pV}/(\text{cm} \cdot \sqrt{\text{Hz}}) \\ \times \left(\frac{3.87 \times 10^{-6} \text{ cm}}{d} \right) \left(\frac{2.14 \times 10^{13} \text{ s}^{-1}}{N_a} \right)^{1/2} \left(\frac{1 \text{ s}}{T} \right)^{1/2} \left(\frac{100 \text{ ns}}{T_2} \right)^{1/2}. \quad (3.41)$$

For instance, we can expect ultimate value $1.7 \text{ fV}/(\text{cm} \cdot \sqrt{\text{Hz}})$ for $T = 10^4$ s. This number can be translated into the GW amplitude $h_{\text{QPNL}} \sim 10^{-23}/\sqrt{\text{Hz}}$. A more efficient way to improve the sensitivity is to use the entanglement of Rydberg atoms. In principle, in the Heisenberg limit, we can improve the sensitivity by $\sqrt{N_a T_2}$. Therefore, in this case, we can expect $h_{\text{QPNL}} \sim 10^{-26}/\sqrt{\text{Hz}}$.

4 Conclusion

We studied high-frequency GWs detectors with Rydberg atoms. First, we showed that a weak electric field signal is generated from the interaction between the GWs and the magnetic field. We calculated the effective electric field induced by the GWs by using improved Fermi-normal coordinates that can incorporate the shorter wavelength of the GWs. We then explained that the weak electric field signal is detected by an electromagnetically induced transparency (EIT) in the system of the Rydberg atoms, and the sensitivity of the Rydberg atoms is further improved by combining the superheterodyne detection method. The point is that the weak signal of the GWs can be measured by the change in the absorption rate of the probe laser that is emitted toward the Rydberg atoms. We showed that the absorption rate is proportional to the imaginary part of electric susceptibility, and that the susceptibility can be related to the density operator of the Rydberg atom. By considering a four-level Rydberg atom that consists of two low energy states $|1\rangle$, $|2\rangle$ and two Rydberg states $|3\rangle$, $|4\rangle$, we obtain the absorption rate in terms of the imaginary part of susceptibility. Then we evaluated the output power of the probe laser and the SNR (signal to noise ratio), that is, the ratio of the output power with a signal of GWs to that with no signal GWs. Using the SNR, we estimated the sensitivity of the GW detector with the Rydberg atoms, i.e., the minimum measurable

value of the electric field when the GWs arrived. Finally, we evaluated the sensitivity of the GW detector with Rubidium Rydberg atoms as an example and found that the sensitivity is $h \sim 10^{-20}$ for 26.4 GHz GWs. We argued that, if the entanglement of atoms could be available, it would be possible to reach $h_{\text{QPNL}} \sim 10^{-26}/\sqrt{\text{Hz}}$ in the future. Therefore, the GWs detector with Rydberg atoms is useful for detecting high-frequency GWs.

One advantage of using the GW detector with Rydberg atom is the availability of quantum entanglement, along with the flexibility to adjust the detector size enabling observation of different frequencies. It is important to perform the detailed analysis to what extent can we utilize entanglement in the detection of gravitational waves.

Acknowledgments

S. K. was supported by the Japan Society for the Promotion of Science (JSPS) KAKENHI Grant Numbers JP22K03621 and JP22H01220. J. S. was in part supported by JSPS KAKENHI Grant Numbers JP20H01902 and JP22H01220. A. T. was supported by Research Support Scholarship from Kuroda Scholarship Foundation.

A Rabi frequency stemming from GWs

When we derive eq. (2.18) and eq. (2.19), we perform integration in spherical coordinates (r, ζ, ϕ) as follows.

For $i = x$, we can calculate as

$$\begin{aligned}
k_k h_{ji}^{\text{TT}} x^j x^k &= k \sin \theta (h_{xx}xx + h_{yx}yx + h_{zx}zx) + k \cos \theta (h_{xx}xz + h_{yx}yz + h_{zx}zz) \\
&= k \sin \theta \left(\frac{h^{(+)}}{\sqrt{2}} \cos^2 \theta xx + \frac{h^{(\times)}}{\sqrt{2}} \cos \theta yx - \frac{h^{(+)}}{\sqrt{2}} \cos \theta \sin \theta zx \right) \\
&\quad + k \cos \theta \left(\frac{h^{(+)}}{\sqrt{2}} \cos^2 \theta xz + \frac{h^{(\times)}}{\sqrt{2}} \cos \theta yz - \frac{h^{(+)}}{\sqrt{2}} \cos \theta \sin \theta zz \right), \quad (\text{A.1})
\end{aligned}$$

and

$$\begin{aligned}
k_i h_{jk}^{\text{TT}} x^j x^k &= k_x h_{xx} x x + k_x h_{yy} y y + k_x h_{zz} z z + 2k_x h_{xy} x y + 2k_x h_{yz} y z + 2k_x h_{zx} z x \\
&= k \sin \theta \left(\frac{h^{(+)}}{\sqrt{2}} \cos^2 \theta x x - \frac{h^{(+)}}{\sqrt{2}} y y + \frac{h^{(+)}}{\sqrt{2}} \sin^2 \theta z z \right. \\
&\quad \left. + 2 \frac{h^{(\times)}}{\sqrt{2}} \cos \theta x y - 2 \frac{h^{(\times)}}{\sqrt{2}} \sin \theta y z - 2 \frac{h^{(\times)}}{\sqrt{2}} \cos \theta \sin \theta z x \right). \quad (\text{A.2})
\end{aligned}$$

When integrating with respect to ϕ in spherical coordinates, terms involving xy, xz, yz will be zero. Thus we obtain

$$\begin{aligned}
h_{0x} &= \omega_g k \left(-\frac{h^{(+)}}{\sqrt{2}} \cos^2 \theta \sin \theta z^2 + \frac{h^{(+)}}{\sqrt{2}} \sin \theta y^2 - \frac{h^{(+)}}{\sqrt{2}} \sin^3 \theta z^2 \right) \left[\frac{\cos(\mathbf{k} \cdot \mathbf{x})}{(\mathbf{k} \cdot \mathbf{x})^2} - \frac{\sin(\mathbf{k} \cdot \mathbf{x})}{(\mathbf{k} \cdot \mathbf{x})^3} \right], \\
&= \omega_g k \frac{h^{(+)}}{\sqrt{2}} \sin \theta (y^2 - z^2) \left[\frac{\cos(\mathbf{k} \cdot \mathbf{x})}{(\mathbf{k} \cdot \mathbf{x})^2} - \frac{\sin(\mathbf{k} \cdot \mathbf{x})}{(\mathbf{k} \cdot \mathbf{x})^3} \right]. \quad (\text{A.3})
\end{aligned}$$

We align the z -axis with the direction of \mathbf{k} and introduce a spherical coordinate system. We then convert the Cartesian coordinate to the spherical coordinate by using $x = r \sin \zeta \cos \phi$, $y = r \sin \zeta \sin \phi$, $z = r \cos \zeta$. Using $\omega_g = k$, $\bar{\epsilon} = k\ell$, $r' = r/\ell$, we can take average

$$\begin{aligned}
\langle h_{0x} \rangle &= \frac{h^{(+)}}{\sqrt{2}} \sin \theta \int_0^1 \int_0^\pi \int_0^{2\pi} dr' d\zeta d\phi r'^2 \sin \zeta \\
&\quad \times (\tan^2 \zeta \sin^2 \phi - 1) \left[\cos(\bar{\epsilon} r' \cos \zeta) - \frac{\sin(\bar{\epsilon} r' \cos \zeta)}{\bar{\epsilon} r' \cos \zeta} \right] \\
&= \frac{h^{(+)}}{\sqrt{2}} \sin \theta F(\bar{\epsilon}), \quad (\text{A.4})
\end{aligned}$$

where we defined

$$\bar{F}(\bar{\epsilon}) \equiv \frac{\pi(\bar{\epsilon}^2 - 12) \text{Si}(\bar{\epsilon})}{4\bar{\epsilon}} + \frac{\pi(\bar{\epsilon}^2 - 30) \cos(\bar{\epsilon})}{4\bar{\epsilon}^2} + \frac{\pi(\bar{\epsilon}^2 + 30) \sin(\bar{\epsilon})}{4\bar{\epsilon}^3}. \quad (\text{A.5})$$

For $i = y$, we can deduce

$$k_i h_{jk}^{\text{TT}} x^j x^k = k_y h_{jk}^{\text{TT}} x^j x^k = 0 \quad (\text{A.6})$$

$$\begin{aligned}
k_k h_{ji}^{\text{TT}} x^j x^k &= k \sin \theta (h_{xy} x x + h_{yy} y x + h_{zy} z x) + k \cos \theta (h_{xy} x z + h_{yy} y z + h_{zy} z z) \\
&= k \sin \theta \left(\frac{h^{(\times)}}{\sqrt{2}} \cos \theta x x - \frac{h^{(+)}}{\sqrt{2}} y x - \frac{h^{(\times)}}{\sqrt{2}} \sin \theta z x \right) \\
&\quad + k \cos \theta \left(\frac{h^{(\times)}}{\sqrt{2}} \cos \theta x z - \frac{h^{(+)}}{\sqrt{2}} y z - \frac{h^{(\times)}}{\sqrt{2}} \sin \theta z z \right). \quad (\text{A.7})
\end{aligned}$$

Again, the cross terms vanish after averaging. Hence, we obtain

$$\begin{aligned}
h_{0y} &= \omega_g k \frac{h^{(\times)}}{\sqrt{2}} \cos \theta \sin \theta (x^2 - z^2) \left[\frac{\cos(\mathbf{k} \cdot \mathbf{x})}{(\mathbf{k} \cdot \mathbf{x})^2} - \frac{\sin(\mathbf{k} \cdot \mathbf{x})}{(\mathbf{k} \cdot \mathbf{x})^3} \right] \\
&= \frac{h^{(\times)}}{\sqrt{2}} \cos \theta \sin \theta (\tan^2 \zeta \cos^2 \phi - 1) \left[\cos(kr \cos \zeta) - \frac{\sin(kr \cos \zeta)}{kr \cos \zeta} \right]. \quad (\text{A.8})
\end{aligned}$$

After the averaging, we have

$$\langle h_{0y} \rangle = \frac{h^{(\times)}}{\sqrt{2}} \cos \theta \sin \theta \bar{F}(\bar{\epsilon}). \quad (\text{A.9})$$

Finally, we obtain

$$\begin{aligned}
\langle \Omega_g \rangle &= \langle \mathbf{d}^{(34)} \cdot \mathbf{E} \rangle = d^{(34)i} \varepsilon^{ijk} \langle h^0_j \rangle B^k \\
&= d_x^{(34)} \langle h_{0y} \rangle B_z - d_y^{(34)} \langle h_{0x} \rangle B_z \\
&= \frac{B_z}{\sqrt{2}} \sin \theta [d_x^{(34)} h^{(\times)} \cos \theta - d_y^{(34)} h^{(+)}] \bar{F}(\bar{\epsilon}). \quad (\text{A.10})
\end{aligned}$$

Note that $\bar{F}(\bar{\epsilon}) = F(\epsilon)$ and $\bar{\epsilon} = 2\pi\epsilon$.

References

- [1] B. P. Abbott et al. ‘‘Observation of Gravitational Waves from a Binary Black Hole Merger’’. In: *Phys. Rev. Lett.* 116.6 (2016), p. 061102. arXiv: 1602.03837 [gr-qc].
- [2] B. P. Abbott et al. ‘‘Prospects for observing and localizing gravitational-wave transients with Advanced LIGO, Advanced Virgo and KAGRA’’. In: *Living Rev. Rel.* 21.1 (2018), p. 3. arXiv: 1304.0670 [gr-qc].
- [3] Pau Amaro-Seoane et al. ‘‘Laser Interferometer Space Antenna’’. In: (Feb. 2017). arXiv: 1702.00786 [astro-ph.IM].
- [4] Naoki Seto, Seiji Kawamura, and Takashi Nakamura. ‘‘Possibility of direct measurement of the acceleration of the universe using 0.1-Hz band laser interferometer gravitational wave antenna in space’’. In: *Phys. Rev. Lett.* 87 (2001), p. 221103. arXiv: astro-ph/0108011.

- [5] Kent Yagi and Naoki Seto. “Detector configuration of DECIGO/BBO and identification of cosmological neutron-star binaries”. In: *Phys. Rev. D* 83 (2011). [Erratum: *Phys.Rev.D* 95, 109901 (2017)], p. 044011. arXiv: 1101.3940 [astro-ph.CO].
- [6] Gabriella Agazie et al. “The NANOGrav 15 yr Data Set: Evidence for a Gravitational-wave Background”. In: *Astrophys. J. Lett.* 951.1 (2023), p. L8. arXiv: 2306.16213 [astro-ph.HE].
- [7] Gabriella Agazie et al. “The NANOGrav 15 yr Data Set: Observations and Timing of 68 Millisecond Pulsars”. In: *Astrophys. J. Lett.* 951.1 (2023), p. L9. arXiv: 2306.16217 [astro-ph.HE].
- [8] Daniel J. Reardon et al. “Search for an Isotropic Gravitational-wave Background with the Parkes Pulsar Timing Array”. In: *Astrophys. J. Lett.* 951.1 (2023), p. L6. arXiv: 2306.16215 [astro-ph.HE].
- [9] Daniel J. Reardon et al. “The Gravitational-wave Background Null Hypothesis: Characterizing Noise in Millisecond Pulsar Arrival Times with the Parkes Pulsar Timing Array”. In: *Astrophys. J. Lett.* 951.1 (2023), p. L7. arXiv: 2306.16229 [astro-ph.HE].
- [10] Andrew Zic et al. “The Parkes Pulsar Timing Array Third Data Release”. In: (June 2023). arXiv: 2306.16230 [astro-ph.HE].
- [11] J. Antoniadis et al. “The second data release from the European Pulsar Timing Array III. Search for gravitational wave signals”. In: (June 2023). arXiv: 2306.16214 [astro-ph.HE].
- [12] J. Antoniadis et al. “The second data release from the European Pulsar Timing Array I. The dataset and timing analysis”. In: (June 2023). arXiv: 2306.16224 [astro-ph.HE].
- [13] J. Antoniadis et al. “The second data release from the European Pulsar Timing Array: V. Implications for massive black holes, dark matter and the early Universe”. In: (June 2023). arXiv: 2306.16227 [astro-ph.CO].
- [14] Heng Xu et al. “Searching for the Nano-Hertz Stochastic Gravitational Wave Background with the Chinese Pulsar Timing Array Data Release I”. In: *Res. Astron. Astrophys.* 23.7 (2023), p. 075024. arXiv: 2306.16216 [astro-ph.HE].

- [15] Kaishu Saito, Jiro Soda, and Hirotaka Yoshino. “Universal 1020 Hz stochastic gravitational waves from photon spheres of black holes”. In: *Phys. Rev. D* 104.6 (2021), p. 063040. arXiv: 2106.05552 [gr-qc].
- [16] Asuka Ito, Kazunori Kohri, and Kazunori Nakayama. “Probing high frequency gravitational waves with pulsars”. In: (May 2023). arXiv: 2305.13984 [gr-qc].
- [17] Asuka Ito and Jiro Soda. “MHz Gravitational Waves from Short-term Anisotropic Inflation”. In: *JCAP* 04 (2016), p. 035. arXiv: 1603.00602 [hep-th].
- [18] Asuka Ito, Jiro Soda, and Masahide Yamaguchi. “Analytic formula for the dynamics around inflation end and implications on primordial gravitational waves”. In: *JCAP* 03 (2021), p. 033. arXiv: 2009.03611 [astro-ph.CO].
- [19] Chiara Caprini and Daniel G. Figueroa. “Cosmological Backgrounds of Gravitational Waves”. In: *Class. Quant. Grav.* 35.16 (2018), p. 163001. arXiv: 1801.04268 [astro-ph].
- [20] Nancy Aggarwal et al. “Challenges and opportunities of gravitational-wave searches at MHz to GHz frequencies”. In: *Living Rev. Rel.* 24.1 (2021), p. 4. arXiv: 2011.12414 [gr-qc].
- [21] Tomotada Akutsu et al. “Search for a stochastic background of 100-MHz gravitational waves with laser interferometers”. In: *Phys. Rev. Lett.* 101 (2008), p. 101101. arXiv: 0803.4094 [gr-qc].
- [22] Asuka Ito et al. “Probing GHz gravitational waves with graviton–magnon resonance”. In: *Eur. Phys. J. C* 80.3 (2020), p. 179. arXiv: 1903.04843 [gr-qc].
- [23] Asuka Ito and Jiro Soda. “A formalism for magnon gravitational wave detectors”. In: *Eur. Phys. J. C* 80.6 (2020), p. 545. arXiv: 2004.04646 [gr-qc].
- [24] Aldo Ejlli et al. “Upper limits on the amplitude of ultra-high-frequency gravitational waves from graviton to photon conversion”. In: *Eur. Phys. J. C* 79.12 (2019), p. 1032. arXiv: 1908.00232 [gr-qc].
- [25] Valerie Domcke, Camilo Garcia-Cely, and Nicholas L. Rodd. “Novel Search for High-Frequency Gravitational Waves with Low-Mass Axion Haloscopes”. In: *Phys. Rev. Lett.* 129.4 (2022), p. 041101. arXiv: 2202.00695 [hep-ph].

- [26] Georg Engelhardt, Amit Bhoonah, and W. Vincent Liu. “Detecting axion dark matter with Rydberg atoms via induced electric dipole transitions”. In: (Apr. 2023). arXiv: 2304.05863 [hep-ph].
- [27] Thomas F Gallagher. “Rydberg atoms”. In: *Springer Handbook of Atomic, Molecular, and Optical Physics*. Springer, 1994, pp. 231–240.
- [28] Christian L Degen, Friedemann Reinhard, and Paola Cappellaro. “Quantum sensing”. In: *Reviews of modern physics* 89.3 (2017), p. 035002.
- [29] Yuan-Yu Jau and Tony Carter. “Vapor-cell-based atomic electrometry for detection frequencies below 1 kHz”. In: *Physical Review Applied* 13.5 (2020), p. 054034.
- [30] Christopher G Wade et al. “Real-time near-field terahertz imaging with atomic optical fluorescence”. In: *Nature Photonics* 11.1 (2017), pp. 40–43.
- [31] Lucy A Downes et al. “Full-field terahertz imaging at kilohertz frame rates using atomic vapor”. In: *Physical Review X* 10.1 (2020), p. 011027.
- [32] Mingyong Jing et al. “Atomic superheterodyne receiver based on microwave-dressed Rydberg spectroscopy”. In: *Nature Physics* 16.9 (2020), pp. 911–915.
- [33] Townes Autler. “Stark Effect in Rapidly Varying Fields”. In: *Phys. Rev. D* 100 (1955), pp. 703–722.
- [34] Michael Fleischhauer, Atac Imamoglu, and Jonathan P. Marangos. “Electromagnetically induced transparency: Optics in coherent media”. In: *Rev. Mod. Phys.* 77 (2005), pp. 633–673.
- [35] PL Fortini and C Gualdi. “Fermi normal co-ordinate system and electromagnetic detectors of gravitational waves. I. Calculation of the metric.” In: *Nuovo Cimento B Serie* 71 (1982), pp. 37–54.
- [36] Karl-Peter Marzlin. “Fermi coordinates for weak gravitational fields”. In: *Phys. Rev. D* 50 (1994), pp. 888–891. arXiv: gr-qc/9403044.
- [37] Malik Rakhmanov. “Fermi-normal, optical, and wave-synchronous coordinates for space-time with a plane gravitational wave”. In: *Class. Quant. Grav.* 31 (2014), p. 085006. arXiv: 1409.4648 [gr-qc].

- [38] Asher Berlin et al. “Detecting high-frequency gravitational waves with microwave cavities”. In: *Phys. Rev. D* 105.11 (2022), p. 116011. arXiv: 2112.11465 [hep-ph].
- [39] Asuka Ito and Jiro Soda. “Exploring High Frequency Gravitational Waves with Magnons”. In: (Dec. 2022). arXiv: 2212.04094 [gr-qc].
- [40] Marlan O Scully and M Suhail Zubairy. *Quantum optics*. 1999.
- [41] Elizabeth J Robertson et al. “ARC 3.0: An expanded Python toolbox for atomic physics calculations”. In: *Computer Physics Communications* 261 (2021), p. 107814.
- [42] Harald Kübler et al. “Coherent excitation of Rydberg atoms in micrometre-sized atomic vapour cells”. In: *Nature Photonics* 4.2 (2010), pp. 112–116.